

Hakan Bozkus
Askin Karakas
Murat Hanci
Mustafa Uzan
Ergun Bozdog
Ali Cetin Sarioglu

Finite element model of the Jefferson fracture: comparison with a cadaver model

Received: 5 July 2000
Revised: 21 December 2000
Accepted: 12 January 2001
Published online: 21 February 2001
© Springer-Verlag 2001

H. Bozkus (✉) · A. C. Sarioglu
Vehbi Koc Foundation American Hospital,
Department of Neurosurgery,
Guzelbahce S 20 80200 Nisantasi,
Istanbul, Turkey
e-mail: bozkus@attglobal.net,
Fax: +90-212-3112190

A. Karakas · E. Bozdog
Faculty of Mechanical Engineering,
Istanbul Technical University,
Istanbul, Turkey

M. Hanci · M. Uzan
Institute of Neurosciences,
Istanbul University, Istanbul, Turkey

Abstract This study tries to explain the reason why the Jefferson fracture is a burst fracture, using two different biomechanical models: a finite element model (FEM) and a cadaver model used to determine strain distribution in C1 during axial static compressive loading. For the FEM model, a three-dimensional model of C1 was obtained from a 29-year-old healthy human, using axial CT scans with intervals of 1.0 mm. The mesh model was composed of 8200 four-noded isoparametric tetrahedrons and 37,400 solid elements. The material properties of the cortical bone of the vertebra were assessed according to the previous literature and were assumed to be linear isotropic and homogeneous for all elements. Axial static compressive loads were applied at between 200 and 1200 N. The strain and stress (maximum shear and von Mises) analyses were determined on the clinically relevant fracture lines of anterior and posterior arches. The results of the FEM were compared with a cadaver model. The latter comprised the C1 bone of a cadaver placed in a methylmethacrylate foam. Axial static com-

pressive loads between 200 and 1200 N were applied by an electrohydraulic testing machine. Strain values were measured using strain gauges, which were cemented to the bone where the clinically relevant fracture lines of the anterior and posterior arches were located. As a result, compressive strain was observed on the outer surface of the anterior arch and inferior surface of the posterior arch. In addition, there was tensile strain on the inner surface of the anterior arch and superior surface of the posterior arch. The strain values obtained from the two experimental models showed similar trends. The FEM analysis revealed that maximum strain changes occurred where the maximum shear and von Mises stresses were concentrated. The changes in the C1 strain and stress values during static axial loading biomechanically prove that the Jefferson fracture is a burst fracture.

Keywords Atlas · Biomechanics · Cervical vertebrae · Finite element analysis · Spinal fracture

Introduction

Anatomically, C1 (the atlas) is embedded in the neck muscles and is therefore not directly subject to any injury. In the Jefferson fracture type of injury, which was first described by Jefferson in 1920 [13], axial loading causes lat-

eral spreading of the lateral masses because of the concave structure of the superior articular facets. The load also affects the anterior-posterior arches, transverse ligament and the dens of C2. The anterior and posterior arches are thin layers of bone, and they are therefore more prone to fracture [5, 23]. This fracture is a type of burst fracture, which bursts into two to four pieces that do not

exert pressure on the spinal cord [1, 3, 8, 11, 14, 16, 17, 18, 26, 29].

The aim of this study is to explain the biomechanical behavior of C1 during Jefferson fracture, using two different biomechanical methods: a finite element model (FEM) and mechanically via strain gauges.

Through the strain and stress results of this study, the authors try to explain why the Jefferson fracture is a burst fracture of two to four pieces, and how it does not cause a neurological deficit.

Materials and methods

Finite element model of C1

A three-dimensional geometric model of C1 was obtained from a 29-year-old healthy human, by using axial computed tomography (CT) scans of 1.0-mm intervals. A Siemens Somatom Plus-S (Erlangen) was used for obtaining the 1.0-mm axial CT scans. The two-dimensional axial C1 CT scans were carried out on personal computers, using a 900 dpi scanner (Agfa Arcus II). The edge detection of images was processed by Corel Draw 6.0 (Corel Corp.) and vectored by AutoCAD V.12 (Autodesk Inc.). A three-dimensional wire frame model of C1 was created using the I-DEAS 4.0 (SDRC). The mesh model of C1 was composed of 8200 four-noded isoparametric tetrahedrons and 37,400 solid elements (Fig. 1). FEM was also applied to this model, using I-DEAS 4.0.

The material properties of the cortical bone of the vertebra, which were obtained from literature (Young's modulus=10,000 MPa, Poisson's ratio=0.29, bone density=0.4(10³) kg/m³), were assumed to be linear isotropic and homogeneous for all elements [12, 24, 39, 40].

The boundary condition of C1 was applied to the anterior and posterior arches, where the atlantoaxial and atlanto-occipital ligaments are attached to the inferior articular facet (IAF) surfaces and to the contact point of the dens of C2. The motion of the model was kept constant in the $\pm y$ direction and free in the $\pm x$ and $\pm z$ directions.

The superior articular facets (SAFs) obtained in the model from CT scans of 1.0-mm axial intervals were flat. Therefore, to simulate the concave shape of the occipital condyles and the convex shape of the SAFs, each of the SAFs was divided horizontally into two equal zones in order to overcome the technical difficulty of applying the load on a non-flat surface. The load was applied at a 15° angle in both the anterolateral and posterolateral orientations on each SAF (Fig. 2).

Axial static compressive loads of 200, 400, 600, 800, 1000 and 1200 N were applied successively to the SAFs. The strain and

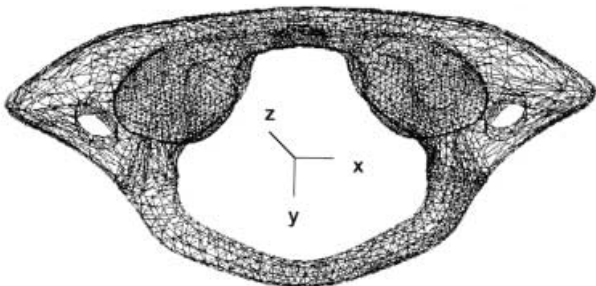


Fig. 1 The mesh model of C1 derived from finite element modeling (FEM)

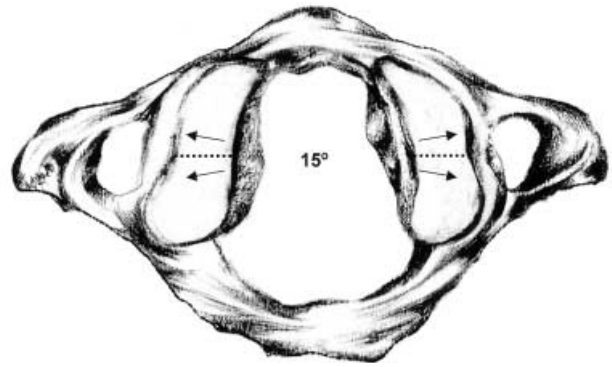


Fig. 2 Schematic representation, using the FEM, of the applied loads with anterolateral and posterolateral angles of 15° on each superior articular facet. (The horizontal dotted lines divide the facet surfaces into two equal zones)

stress analyses of clinically relevant fracture lines under these loads were performed on the anterior and posterior arches. The strain, maximum shear stress and von Mises stress were calculated and compared to each other.

Finally, the experimental validation was made through a comparison of the strain results with those of the cadaver model.

Cadaver model of C1

The C1 vertebra of a man who had died of an ischemic heart attack 9 months previously at the age of 39 was extracted for testing the biomechanical data of the model. All adhering soft tissues were removed from the bone, and the periosteal membrane of the bone was resected to allow placement of the strain gauges.

The cadaver model and FEM were taken from different specimens in order to illustrate the applicability of the FEM to patient-specific anatomical variations.

Six strain gauges were used. Four of them were cemented to the surface of the bone, across the clinically relevant fracture lines on the inner-outer surfaces of the anterior arch (in the $\pm y$ plane) and the superior-inferior surfaces of the posterior arch (in the $\pm x$ plane) perpendicularly, using cyanoacrylic adhesive material. The remaining two were cemented onto the outer surface of the anterior arch and the superior surface of the posterior arch respectively, parallel to the clinically relevant fracture lines (Fig. 3). The strain gauges used (HBM, Spectris Messtechnik GmbH) have the following properties: a gauge resistance of 120 Ω , a gauge factor of 2.05 and a gauge length of 4 mm. These gauges were connected to a data logger (TEC- equipment E31-MKIII strain bridge), which included an RS-232 data acquisition card. The voltage changes in each strain gauge were converted into units of microstrain ($\mu\epsilon$), which were then printed.

The upper and lower surfaces of the bone were separately embedded in methylmethacrylate foam, so as to obtain a positive model, and later these positive models were embedded in methylmethacrylate foam in order to obtain negative models. One of these negative models represented the occipital condyle and the other represented the SAFs of C2. C1 was placed between these negative models in a neutral position to achieve the greatest occiput-C1-C2 articular congruency. Sponges, which were placed at certain points between the bone and the negative models in order to simulate the dens of C2 and the anterior-posterior atlanto-occipital and atlantoaxial membranes, were used to give mobile flexibility. The bone between these two negative models was put in an electrohydraulic material testing machine (Universal Material Testing Machine Model/ Serial no: SM 100/ J, 1007/ 4, Tecquip-

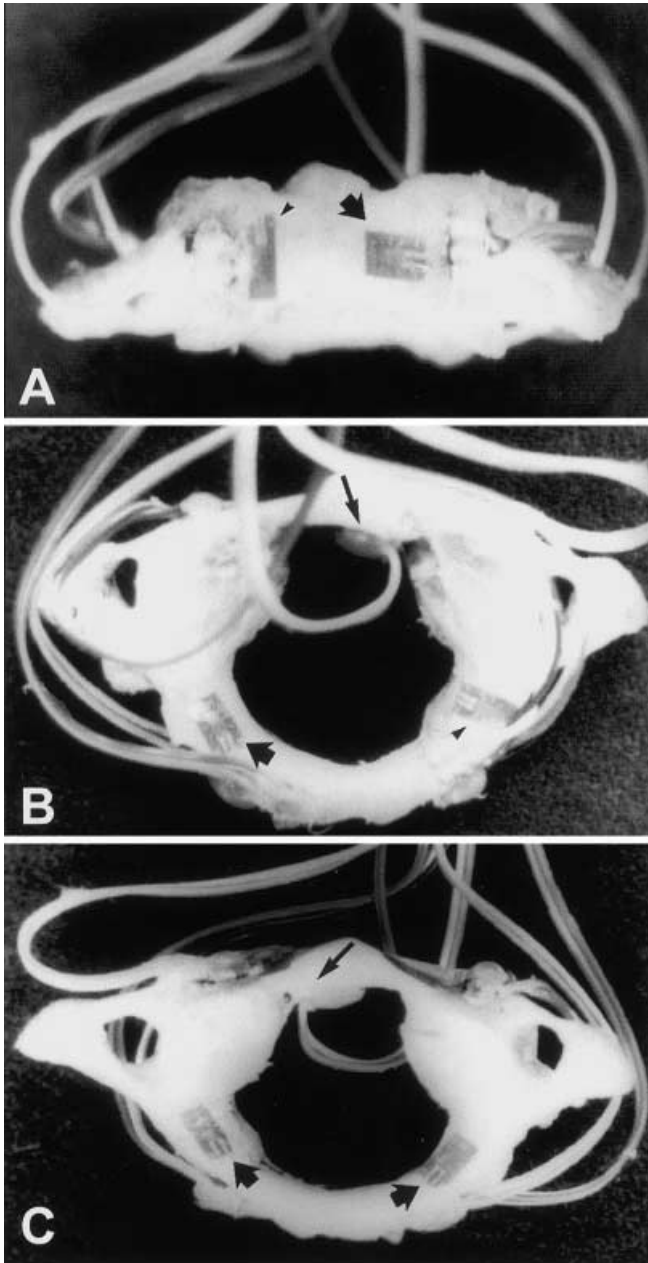


Fig. 3A–C Photograph of a cadaver C1 bone. Strain gauges were cemented on clinically relevant fracture lines of the bone at the following sites: **A** the outer surface of the anterior arch, in the $\pm y$ plane (on the right – *arrow* – perpendicular, and on the left – *arrow head* – parallel); **B** the superior surface of the posterior arch, in the $\pm x$ plane (on the right – *arrow head* – parallel, and on the left – *arrow* – perpendicular) and on the inner surface of the anterior arch, in the $\pm y$ plane (*long arrow*, perpendicular); and **C** the inferior surface of the posterior arch, in the $\pm x$ plane (*both arrows*, perpendicular) and on the inner surface of the anterior arch, in the $\pm y$ plane (*long arrow*, perpendicular)

ment Ltd.). The axial static loads of 200, 400, 600, 800, 1000 and 1200 N were applied upon the upper negative model at a rate of 0.5 mm/min.

The strain from each gauge was converted into tensile and compressive components. The tensile strain expresses the ratio of the extended length of the bone surface, and the compressive strain expresses the ratio of the shrunken length of the bone surface at the site of the gauge.

Results

Results of the finite element model testing

The results of the three-dimensional FEM of C1 obtained from axial static loads of 200, 400, 600, 800, 1000 and 1200 N were categorized as the strain, maximum shear stress and von Mises stress.

The strain distribution was recorded in the $\pm y$ plane of the outer and inner surface of the anterior arch, and the $\pm x$ plane of the superior and inferior surface of the posterior arch, where the clinically relevant fracture lines occur. Whereas the strain range on the outer surface of the anterior arch was between -54×10^{-6} and -330×10^{-6} , on the inner surface of the anterior arch it was between 118×10^{-6} and 561×10^{-6} . On the other hand, the strain range on the superior surface of the posterior arch was between 174×10^{-6} and 482×10^{-6} , while on the inferior surface of the posterior arch it was between -45×10^{-6} and -273×10^{-6} .

The maximum shear stress was recorded on the anterior arch as between 0.48 and 3.26 MPa, and between 0.30 and 2.18 MPa on the posterior arch. Finally, the von Mises stress was observed to be between 0.90 and 5.80 MPa on the anterior arch, and between 0.70 and 4.84 MPa on the posterior arch.

Both maximum shear stress and von Mises stress concentrated on the same location of the bone, where the maximum strain differences occurred. These points are also the sites of clinically observed fracture lines (Fig. 4).

Results of the cadaver model testing

The strain distribution in the cadaver model of C1 during the static axial loading of 200, 400, 600, 800, 1000 and 1200 N was recorded on the $\pm y$ plane of the outer and inner surface of the anterior arch, and the $\pm x$ plane of superior and inferior surfaces of the posterior arch, where the clinically relevant fracture lines occurred, using strain gauges.

The strain range on the outer surface of the anterior arch was between -73×10^{-6} and -387×10^{-6} , whereas on the inner surface of the anterior arch it was between 103×10^{-6} and 488×10^{-6} . The strain range on the superior surface of the posterior arch was between 124×10^{-6} and 453×10^{-6} , and between -89×10^{-6} and -303×10^{-6} on the inferior surface of the posterior arch.

The results obtained from the strain gauges cemented on the surfaces of the anterior and the posterior arches,

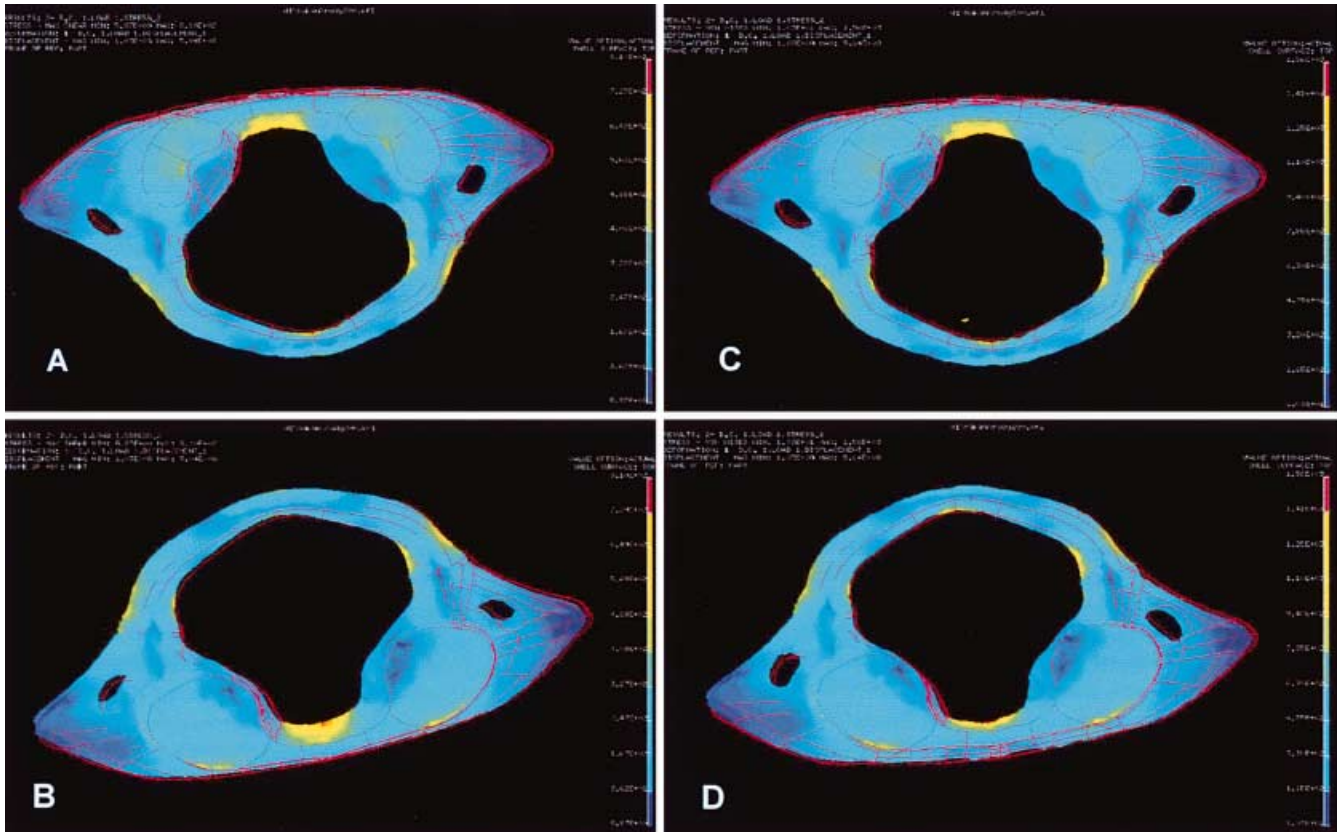


Fig. 4A–D Photograph shows the distribution of maximum shear stress (*on the left*) and von Mises stress (*on the right*) after 200 N axial static compressive loading on C1 in FEM. **A,C** Superior view of the bone, **B,D** inferior view of the bone. The *color scale* on the right represents the scale of stress, from the highest at the top to the lowest at the bottom

perpendicular to clinically relevant fracture lines (Fig. 3), are presented here as a representative validation of the FEM.

The strain results obtained from both studies indicated that the highest tensile strain values were recorded on the inner surface of the anterior arch and the superior surface of the posterior arch, whereas the greatest compressive strain was recorded on the outer surface of the anterior arch and the inferior surface of the posterior arch (Fig. 5, Fig. 6).

As explained above, the strain values of the cadaver model are in the same range as those of the FEM. The strain results of both models were noted to show a similar trend (Fig. 7).

Discussion

Biomechanical spine studies have been carried out in various ways (animal, cadaver and analytical models) [6, 7, 12, 19, 21, 22, 23, 25, 27, 33, 34, 36, 38], but in the last two decades, FEM, of which the application to the cervi-

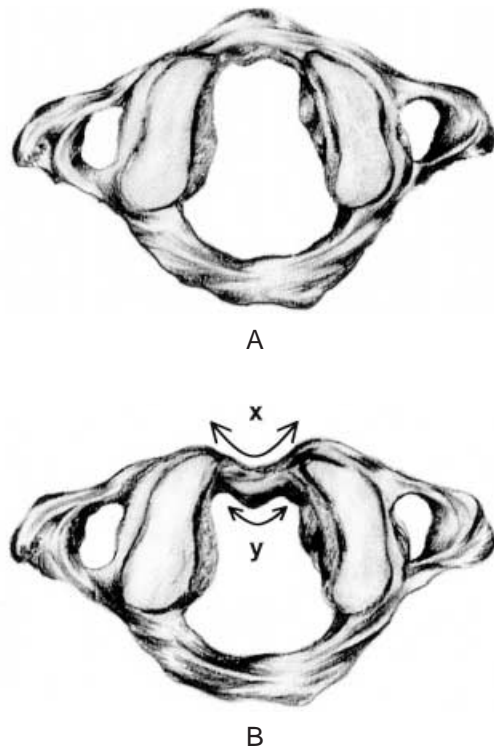


Fig. 5A,B Exaggerated schematic drawings illustrating strain differences in both of the experimental studies on the anterior arch (*x* is compressive strain, *y* is tensile strain). **A** Normal axial position of C1. **B** Position after axial static compressive loading

cal spine was first performed by Yoganandan et al. [15, 32, 38, 39, 40], has become popular in spinal biomechanical research [4, 9, 15, 20, 24, 26, 30, 32, 35, 38, 39, 40].

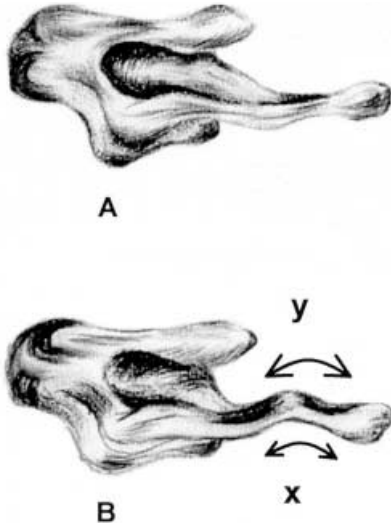
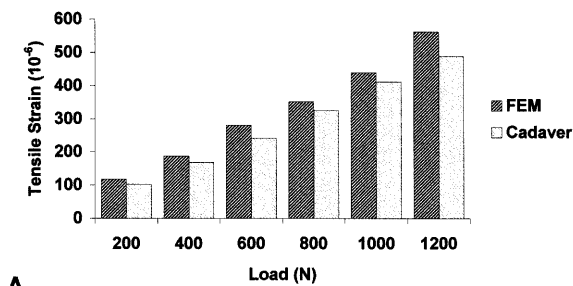
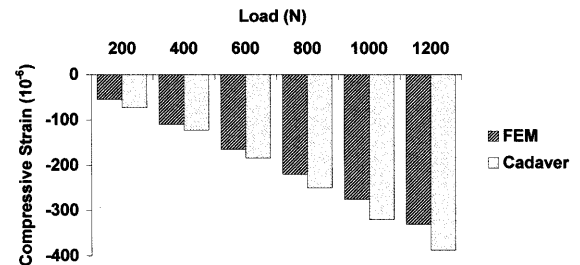


Fig. 6A,B Exaggerated schematic drawings illustrating strain differences in both of the experimental studies on the posterior arch (x is compressive strain, y is tensile strain). **A** Normal lateral position of C1. **B** Position after axial static compressive loading

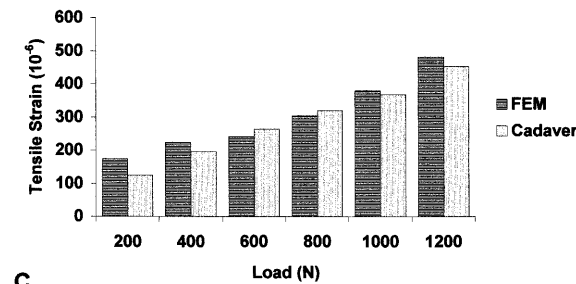
Fig. 7 Bar graphs depicting the strain values in both of the studies, showing the tensile strain distribution on the inner surface of the anterior arch (A) and on the superior surface of the posterior arch (C), and the compressive strain distribution on the outer surface of the anterior arch (B), and on the inferior surface of the posterior arch (D)



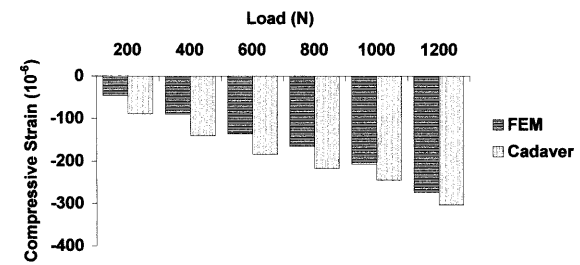
A



B



C



D

In this paper, the results of tests on the FEM and the cadaver model are compared and discussed in the light of the findings of previous literature.

For the three-dimensional modeling of C1, the first step is obtaining an accurate geometric model. If the C1 model is obtained by 1-mm-interval axial CT scans, it is observed that the SAFs and IAFs are flat. However, in the real anatomical nature, the SAFs are smooth, slightly concave, oval or kidney-shaped, and face inward and upward to support the occipital condyles with which they articulate. The IAFs are flatter and more circular, facing caudally and inward to articulate with the SAFs of C2. Detailed information on the anatomical structure of the SAFs from the reports of Singh [28], Tulsi [31] and Gottlieb [10] show that the outlines of SAFs often have constrictions in the middle and cause the shape to look like the figure 8. These constrictions can completely divide the facet surface. The depth of SAFs can vary from being flat – 3 mm or less – to 5 mm or greater [31]. The condyles of the occiput roll backward and slide slightly posteriorly on the SAFs, while the SAFs roll anteriorly and superiorly on the occiput to produce 10° of flexion. The converse action produces 15° of extension [23]. Consequently, the fact that we divided each of the SAFs horizontally into two zones, because of technical problems, actually suits the anatomical nature of the structure.

Moreover, because the range of motion of atlanto-occipital articulation is between 10° flexion and 15° extension, the loading in the study was applied on the two separate zones of SAFs at anterolateral and posterolateral angles of 15° each, to simulate the occipital condyles' shape.

Generally, the axial dynamic loads that cause bone or ligament injury in cervical models are approximately

500–700 N [6, 19, 36, 37]. However, in head models, it is between 3000 and 17,000 N [6, 34].

An experimental study of a Jefferson fracture in the cadaver trauma model has recently been published by Beckner et al. [2]. According to this report, a two- or three-piece Jefferson fracture was caused by dynamic axial loading in intact and ruptured transverse ligament specimens. The authors state that the load range for fractures in both specimens (with/without transverse ligament) is between 980 and 3773 N.

In this study, the axial loads applied to the models were chosen to be within the range of 200–1200 N, reflecting the values that cause transverse ligament rupture in the literature [2, 29].

However, the purpose of using static loading instead of dynamic loading is to analyse the strain and stress at the clinically relevant point of fracture on the bone, by gradually increasing the load, rather than to fracture the bone, which is a possible outcome of dynamic loading.

Considering the fact that the cancellous content of C1, theoretically from a mechanical perspective, can be disregarded in comparison with its cortical content [5], in our model the material properties of C1 were defined as those of a cortical bone without applying mesh partition. Therefore, the material properties of the cortical bone were defined as linear isotropic and homogeneous.

It is worth noting that a midline sagittal cut of C1 shows that the superior-inferior diameter of the anterior arch is longer than that of the posterior arch, whereas its anterior-posterior diameter is narrower than that of the posterior arch [5]. In the light of this observation, it is assumed that the fracture on the anterior arch will be in the $\pm z$ plane, whereas it will be in the $\pm y$ plane on the posterior arch. Therefore, in the cadaver model, the strain gauges were cemented onto the clinically relevant fracture lines in a perpendicular orientation ($\pm y$ plane on the anterior arch, $\pm x$ plane on the posterior arch), in order to ensure that the maximum changes in the strain values could be readily recorded.

The advantage of the FEM study is that the maximum shear stress and von Mises stress can be recorded as well. In addition, the stresses are concentrated primarily at the points where the maximum strain differences (either negative or positive) occurred.

If the location of C1 within the upper cervical complex and the quantitative results of these experimental studies are evaluated together, the biomechanical behavior of C1 during a burst fracture can be explained in the following way. Because the strain differences cause compressive strain on the outer surface of the anterior arch and tensile strain on its inner surface, the anterior arch is liable to bend towards the spinal canal. However, this inward

bending motion of the anterior arch is prevented by the dens of C2. The evidence for this is that the stress values increase at the point where the dens contacts the anterior arch. This could conceivably explain the uncommon, but difficult to explain, association of unstable Jefferson fractures with type II odontoid fractures. On the other hand, the strain differences cause tensile strain on the superior surface of the posterior arch and compressive strain on its inferior surface. Most probably, the downward motion of the posterior arch is prevented by the spinous process of C2. This, in turn, can be proved by the concentration of stresses at the points where the maximum strain differences occur at the posterior arch. It might be suggested that this is the reason why the burst fracture of C1 does not cause any injuries to the spinal cord.

Moreover, the fact that strain results obtained from the anterior and posterior arches displayed similar ranges may show that they react similarly to axial loading in terms of resistance, and this may explain why a Jefferson fracture is a burst fracture of two to four pieces.

Taking into consideration the relation between the anterior arch, the odontoid process and the transverse ligament, the results of this study – although they do not provide an exact approach to the treatment of Jefferson fractures – may suggest that in unstable Jefferson fractures, observed in combination with type II odontoid fractures, rigid fixation would be a better alternative for treatment.

This study should be regarded as a prototype for FEM applications on the upper cervical unit. The next step could be a nonlinear analysis, through applying dynamic loads and defining the occipital bone, C2 and relevant ligaments.

Conclusion

The fact that the strain results (through FEM and the cadaver model) and the stress values (through FEM only), obtained from the clinically relevant points of the anterior and posterior arches during static axial compressive loading on C1 show similar trends and ranges is further evidence, in biomechanical terms, that the Jefferson fracture is indeed a burst fracture.

Acknowledgements The authors are grateful for the invaluable help and suggestions of Professor Narayan Yoganandan, Department of Biomechanics, Medical College of Wisconsin; Professor Civan Islak, Department of Radiology, Istanbul University, Cerrahpasa Medical School; and Professor Edward C. Benzel, Department of Neurosurgery, Cleveland Clinic Foundation, for their scholarly contributions, and Bahar Yildirim for her contributions to the English translation of the article.

References

1. Allen BL, Ferguson RL, Lehmann TR, et al (1982) A mechanistic classification of closed, indirect fractures and dislocations of the lower cervical spine. *Spine* 7:1–27
2. Beckner MA, Heggeness MH, Doherty BJ (1998) A biomechanical study of Jefferson fractures. *Spine* 23:1832–1836
3. Bohlman HH (1979) Acute fractures and dislocations of the cervical spine. *J Bone Joint Surg Am* 61:1119–1141
4. Bozic KJ, Keyak JH, Skinner HB, et al (1994) Three-dimensional finite element modeling of a cervical vertebra: an investigation of burst fracture mechanism. *J Spinal Disord* 7:102–110
5. Brian JD, Michael HH (1994) The quantitative anatomy of the atlas. *Spine* 19:2497–2500
6. Crowell RR, Edwards WT, White AA (1989) Mechanisms of injury in the cervical spine: experimental evidence and biomechanical modeling. In: Sherk HH (ed) *The cervical spine*. JB Lippincott, Philadelphia, pp 70–90
7. Deng YC, Goldsmith W (1987) Response of a human head/neck/upper torso replica to dynamic landing. II. Analytic/numerical model. *J Biomech* 20: 487–493
8. Fowler JL, Sandhu A, Fraser RD (1990) A review of fractures of the atlas vertebra. *J Spinal Disord* 3:19–24
9. Gilbertson LG, Goel VK, Kong WZ, Clausen JD (1995) Finite element methods in spine biomechanics research. *Crit Rev Biomed Eng* 23:411–473
10. Gottlieb MS (1994) Absence of symmetry in superior articular facets on the first cervical vertebra in humans: implications for diagnosis and treatment. *J Manipulative Physiol Ther* 17:314–320
11. Hadley MN, Dickman CA, Browner CM, et al (1988) Acute traumatic atlas fractures: management and long term outcome. *Neurosurgery* 23:31–35
12. Hakim N, King A (1979) A three dimensional finite element dynamic response analysis of a vertebra with experimental verification. *J Biomech* 12:277–292
13. Jefferson G (1920) Fracture of the atlas vertebra. Report of four cases, and a review of those previously recorded. *Br J Surg* 7:407–422
14. Kesterson L, Benzel E, Orrison W, et al (1991) Evaluation and treatment of the atlas burst fractures (Jefferson fractures). *J Neurosurg* 75:213–220
15. Kumaresan S, Yoganandan N, Pintar FA, et al (1997) Finite element modeling of cervical laminectomy with graded facetectomy. *J Spinal Disord* 10:40–46
16. Landells CD, van Peteghem PK (1988) Fractures of the atlas: classification, treatment and morbidity. *Spine* 13: 450–452
17. Levine AM, Edwards CC (1986) Treatment of injuries in the C1–C2 complex. *Orthop Clin North Am* 17:31–44
18. Levine AM, Edwards CC (1991) Fractures of the atlas. *J Bone Joint Surg Am* 73:680–691
19. Maiman DJ, Sances A, Myklebust JB, et al (1983) Compression injuries of the cervical spine; a biomechanical analysis. *Neurosurgery* 13: 254–260
20. Natali A, Meroi E (1990) Nonlinear analysis of intervertebral disk under dynamic load. *J Biomech Eng* 112: 358–362
21. Panjabi MM (1973) Three dimensional mathematical model of the human spine structure. *J Biomech* 6:761–767
22. Panjabi M, Dvorak J, Duranceau J, et al (1988) Three dimensional movements of the upper cervical spine. *Spine* 13:726–730
23. Panjabi MM, Oda T, Crisco JJ III, et al (1991) Experimental study of atlas injuries. Biomechanical analysis of their mechanisms and fracture patterns. *Spine* 16:S460–S465
24. Saito T, Yamamuro T, Shikata J, et al (1991) Analysis and prevention of spinal column deformity following cervical laminectomy; pathogenic analysis of postlaminectomy deformities. *Spine* 16:495–502
25. Sanan A, Rengachary SS (1996) The history of spinal biomechanics. *Neurosurgery* 39:657–669
26. Schlicke LH, Callahan RA (1981) A rational approach to burst fractures of the atlas. *Clin Orthop* 154:18–21
27. Shah JS, Hampson WGJ, Jayson MIV (1978) The distribution of surface strain in the cadaveric lumbar spine. *J Bone Joint Surg Br* 60:246–251
28. Singh S (1965) Variations of the superior articular facets of atlas vertebrae. *J Anat* 99:565–571
29. Spence KF (1970) Bursting atlantal fracture associated with rupture of the transverse ligament. *J Bone Joint Surg Am* 52:543–549
30. Teo E, Paul JP, Evans JH (1994) Finite element stress analysis of a cadaver second cervical vertebra. *Med Biol Eng Comput* 32:236–238
31. Tulsi RS (1978) Some specific anatomical features of the atlas and axis: dens, epitransverse process and articular facets. *Aust N Z J Surg* 48:570–574
32. Voo LM, Kumaresan S, Yoganandan N, et al (1997) Finite element analysis of cervical facetectomy. *Spine* 22:964–969
33. Williams JL, Belytschko TB (1983) A three-dimensional model of human cervical spine for impact simulation. *J Biomech Eng* 105:321–331
34. Yoganandan N, Sances A, Maiman D, et al (1986) Experimental spinal injuries with vertical impact. *Spine* 11: 855–860
35. Yoganandan N, Myklebust JB, Ray G, et al (1987) Mathematical and finite element analysis of spine injuries. *Crit Rev Biomed Eng* 15:29–91
36. Yoganandan N, Sances A, Pintar FA (1989) Biomechanical evaluation of the axial compressive responses of the human cadaveric and manikin necks. *J Biomech Eng* 111:250–255
37. Yoganandan N, Sances A, Pintar F, et al (1990) Injury biomechanics of the human cervical column. *Spine* 15: 1031–1039
38. Yoganandan N, Kumaresan SC, Voo L, et al (1996) Finite element application in human cervical spine modeling. *Spine* 21:1824–1834
39. Yoganandan N, Kumaresan SC, Voo L, et al (1996) Finite element modeling of the C4–C6 cervical spine unit. *Med Eng Phys* 18:569–574
40. Yoganandan N, Kumaresan S, Voo L, et al (1997) Finite element model of the human lower cervical spine: parametric analysis of the C4–C6 unit. *J Biomech Eng* 119:87–92